International Journal of Nanomedicine

Dovepress
Taylor & Francis Group

Open Access Full Text Article

ORIGINAL RESEARCH

LIPUS Responsive Dopamine-Modified PVDF Piezoelectric Nanofiber Membrane for Full-Thickness Skin Wound Healing

Zhiying Zhang[1,*], Lijun Liu[1,*], Huan Wang[2,*], Wangni Xie[1], Wenhao Zhai[1], Linlin Wen[1], Boya Zhang[1], Kexuan Liu[1], Xue Zhang[1], Shuchen Liu[1], Lei Huang[1], Daowei Li[1], Yanmin Zhou[1]

[1]Jilin Provincial Key Laboratory of Tooth Development and Bone Remodeling, Hospital of Stomatology, Jilin University, Changchun, 130021, People's Republic of China; [2]State Key Laboratory of Rare Earth Resources Utilization and Laboratory of Chemical Biology, Changchun Institute of Applied Chemistry, Chinese Academy of Sciences, Changchun, 130022, People's Republic of China

*These authors contributed equally to this work

Correspondence: Daowei Li; Yanmin Zhou, Email jluldw@jlu.edu.cn; Zhouym@jlu.edu.cn

Objective: Large full-thickness skin wounds pose significant challenges, particularly in achieving scar-free healing and the regeneration of skin appendages. This study introduces a portable approach for promoting scarless healing and skin appendage regeneration by utilizing low-intensity pulsed ultrasound (LIPUS) activated piezoelectric electrospun membranes to modulate the local electrical environment.

Methods: Dopamine-modified polyvinylidene fluoride (DA/PVDF) nanomembranes were fabricated via electrospinning, followed by piezoelectric characterization under varying LIPUS stimulation. Cell adhesion was examined using SEM and laser confocal microscopy to assess surface interactions. Cell proliferation and migration were further analyzed using the CCK-8 assay and Transwell migration assay, respectively. Finally, the effects of DA/PVDF membranes on full-thickness skin defect healing were tested in a mouse model. The healing process was documented with photographs, and functional skin regeneration was evaluated through histological analysis.

Results: The DA/PVDF nanomembranes had an average diameter of 732 ± 232 nm and generated a voltage of 450 mV under LIPUS stimulation, a 1.28-fold increase compared to PVDF membranes alone. In vitro, LIPUS-activated membranes enhanced cell adhesion and proliferation, resulting in a 1.14-fold increase in cell growth over three days. The transwell migration assays showed 244.67 ± 7.85 migrated cells. *In vivo*, the DA/PVDF+LIPUS group exhibited significantly higher wound healing rates, with improved epidermal regeneration, collagen fiber deposition and remodeling, and enhanced blood vessel and skin appendage formation.

Conclusion: DA modification enhances the piezoelectric properties of PVDF membranes, boosting cell adhesion and promoting dermal and vascular regeneration. LIPUS-generated mechanical waves effectively stimulate membrane deformation, producing a localized electrical microenvironment that mimics the natural bioelectric field of skin and accelerates functional wound healing.

Keywords: piezoelectric materials, dopamine, low-intensity pulsed ultrasound, skin wound healing, skin appendage regeneration

Introduction

The skin, as the body's largest organ, exhibits heightened susceptibility and vulnerability to external threats.[1] Skin wound repair constitutes an intricate and continuously dynamic process, encompassing hemostasis, inflammation, proliferation, and remodeling.[2] Various wound dressings have been developed to treat different wound types, categorized by forms like gauze, hydrogels, and foams.[3–5] Nevertheless, contemporary wound dressings primarily prioritize reducing infection and rehydrating tissue, thereby creating a passive healing environment. A passive healing environment often proves challenging to re-regulate given the dynamic nature of the healing process once the wound dressing has been applied.[6,7] Therefore, there is still an urgent need for the development of more effective and real-time controllable treatments that promote skin regeneration.

Received: 17 October 2024
Accepted: 15 April 2025
Published: 1 May 2025

Graphical Abstract

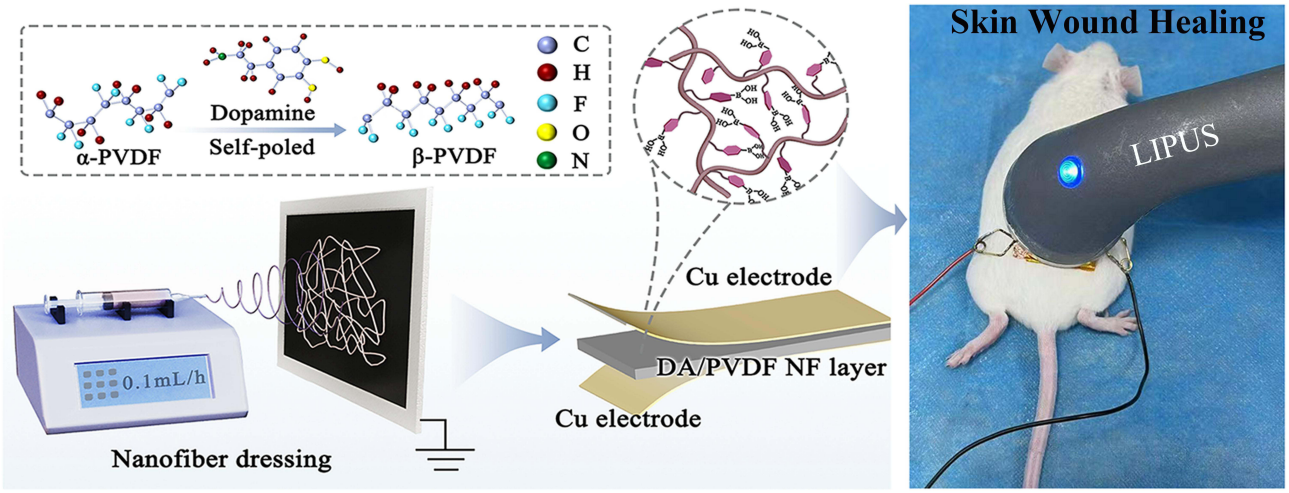

Inspired by the endogenous electric fields generated during skin injury in living organisms, Electrical Stimulation (ES) therapy has garnered much attention in recent years for its safety, simplicity, and controllability.[8] ES has shown potential in enhancing all phases of wound healing, improving cell behavior by promoting glial cell and fibroblast proliferation and differentiation.[9] However, current clinical ES devices rely on external electrodes and wires, making them costly, cumbersome, and unsuitable for home use. Therefore, a non-invasive, wireless system capable of real-time modulation of cell behavior is needed for effective and convenient wound healing.

Piezoelectric materials, which generate localized electrical stimulation through self-deformation, offer a promising solution for tissue repair independent of external power sources.[10] Among these materials, Polyvinylidene fluoride (PVDF) has gained significant attention in wound management due to its biocompatibility, flexibility, and cost-effectiveness.[11] To address potential depolarization and improve the super hydrophobicity of PVDF, various chemically and biologically active molecules have been used for modification.[12,13] For instance, Du et al developed a wound dressing combining hydrogel (PDA-PAAm) and PVDF nanofibers, where body-induced piezoelectricity accelerated full-thickness skin wound healing, reducing closure time by about 33%.[12] Fu reported a polyacrylonitrile/poly (vinylidene fluoride) (PAN-PVDF) hydrogel as a biomimetic skin substitute, where dipolar interactions between PVDF and PAN enhanced the electroactive β-phase, improving the piezoelectric effect.[13] Dopamine (DA), a molecule structurally similar to mussel adhesion proteins, has been used to modify material surfaces, enhancing hydrophilicity and biocompatibility.[14–16] Recent study have shown that DA could enhance and stabilize piezoelectric properties of PVDF by promoting β-phase formation.[17] Despite advancements, PVDF membranes in wound sites often lack sufficient mechanical stimulation and deformation, leading to suboptimal piezoelectric effects and inadequate wound healing. Additionally, the application of these membranes in wound healing has not been thoroughly explored. FDA-approved since 1994, Low-Intensity Pulsed Ultrasound (LIPUS) has shown promising results in healing soft tissues and is well-suited for home-based rehabilitation.[18–21] LIPUS presents a versatile solution by delivering mechanical waves that stimulate piezoelectric materials, creating localized electrical fields at the wound site.[22]

In this study, we developed a novel strategy for skin wound healing by combining LIPUS with piezoelectric electrospun membranes. The mechanical waves generated by LIPUS effectively stimulate membrane deformation, which in turn generates sufficient electrical current. This LIPUS-activated membrane creates a localized electrical microenvironment, mimicking a bioelectric field of skin that promotes wound healing. In vitro assays showed that DA/PVDF membranes, especially when stimulated by LIPUS, significantly improved cell adhesion compared to conventional PVDF. Moreover, LIPUS-activated DA/PVDF membranes accelerated cell proliferation and migration, facilitating faster wound healing. In vivo experiments using a mouse model confirmed the efficacy of LIPUS-activated DA/PVDF membranes in promoting full-thickness skin wound

regeneration. Histological analysis at day 14 revealed superior angiogenesis and skin appendage formation in the DA/PVDF + LIPUS group compared to other treatments. Notably, this group showed a well-organized dermis with minimal excessive collagen deposition, indicating effective tissue remodeling. These findings demonstrate the potential of LIPUS-activated DA/PVDF membranes for advancing wound healing therapies. By combining the benefits of piezoelectric materials and LIPUS, our approach offers a promising strategy for improving skin regeneration and tissue repair.

Materials and Methods

Reagents and Materials

PVDF powder (MW = 5.34 kDa), Dopamine hydrochloride (DA 98%) as purchased by McLean Biochemicals Ltd. Inc. Acetone (99.5%), N,N-dimethylformamide (DMF, 99.8%), were purchased from Aladdin. The Low-Intensity Pulsed Ultrasound (LIPUS) was transmitted through coupling gel (Jinya Inc., China). Dulbecco's modified Eagle's medium (DMEM), fetal bovine serum (FBS), and PBS were obtained from Gibco (Grand Island, USA). Rhodamine and 4',6-diamino-2-phenylindole were purchased from Solabio (Beijing, China). All chemicals are of analytical purity and can be used without further purification.

Cell Culture

Murine fibroblast cell line L929 (American Type Culture Collection, ATCC, Rockville, MD, US) was maintained in DMEM supplemented with FBS (10%) and penicillin-streptomycin (1%) at 37°C in a humidified incubator containing 5% carbon dioxide.

The Preparation of Piezoelectric DA/PVDF Nanofiber Membranes

The preparation of DA/PVDF nanofiber membranes and PVDF nanofiber membranes is shown schematically in Figure 1a, Video S1 and Video S2. DA and PVDF were mixed at different weight fractions. The mixture was dissolved

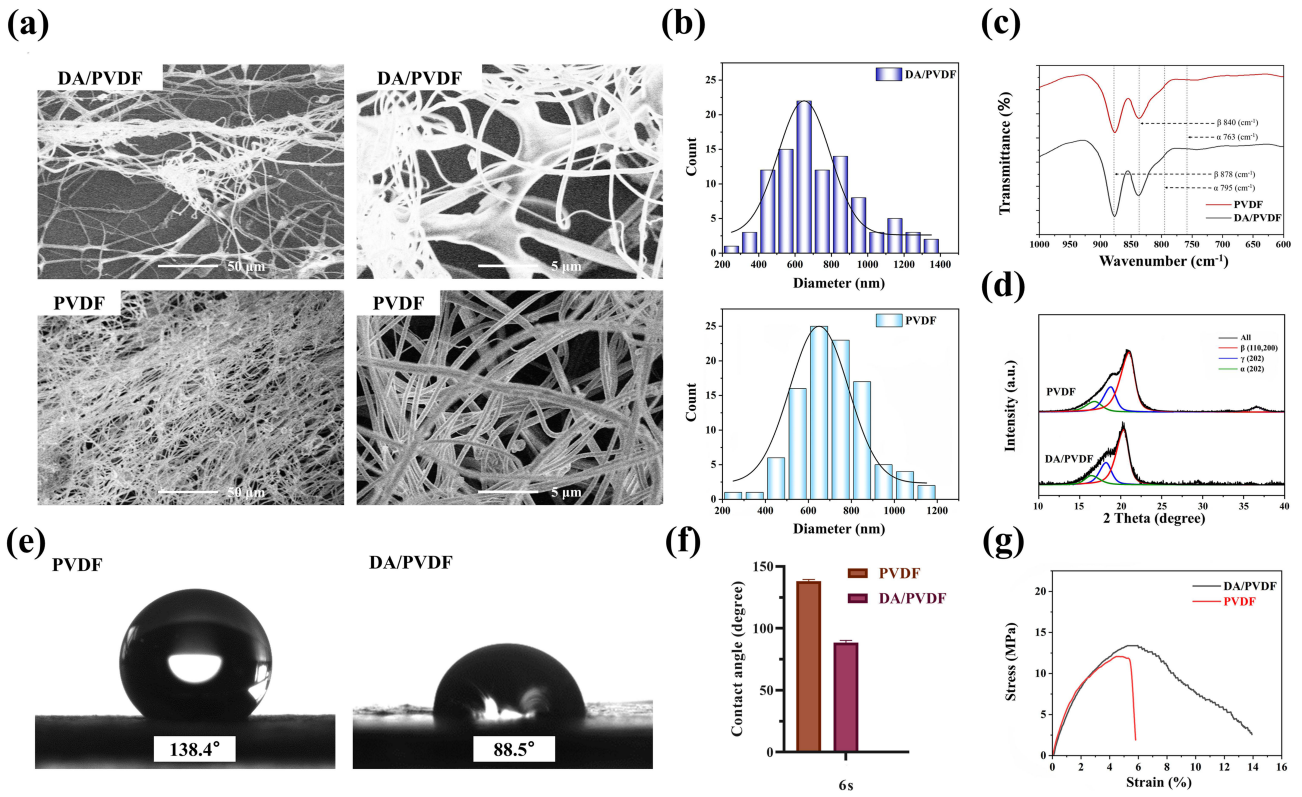

Figure 1 Characterization of the DA/PVDF membrane. (**a**) Microstructure of PVDF and DA/PVDF membranes. (**b**) Diameter distribution of PVDF nanofiber membranes and DA/PVDF nanofiber membranes. (**c**) FTIR spectra of PVDF nanofiber membranes and DA/PVDF nanofiber membranes with 1.0 wt% DA loading content. (**d**) XRD spectra of PVDF nanofiber membranes and DA/PVDF nanofiber membranes with 1.0 wt% DA loading content. (**e**) The water contact angle (WCA) of PVDF and DA/PVDF membrane. (**f**) Quantitative contact angle data of PVDF and DA/PVDF membranes. (**g**) Typical tensile stress–strain curves of PVDF and DA/PVDF membranes.

https://doi.org/10.2147/IJN.S496921

in 3:7 (w/w) acetone/N, N-dimethylformamide (DMF) solvent and sonicated for 90 min, followed by stirring with a magnetic stirrer using a polygonal magnetic stir bar at 500 rpm for 12 h. A homogenized DA/PVDF solution with a concentration of 15 wt% was obtained. We injected the mixed solution into a syringe with a distance of 15 cm between the spinneret and the collector. The electrostatic spinning process was conducted using a high direct current voltage of 18 kV with a solution flow speed at 1 mL/h at room temperature and 35% humidity. The prepared DA/PVDF nanofiber membranes were dried 2 weeks at room temperature. In the in vitro cell culture assay, the cell membranes were irradiated under UV light for 30 min and then sterilized in 75% ethanol solution for 30 min.

Characterization

The chemical composition was assessed by Fourier transform infrared spectroscopy (FT-IR, Bruker Vertex 80v, Germany). In order to investigate the effect of dopamine on the properties of electrospun PVDF nanofiber membranes, we performed XRD analysis (XRD, Rigaku D/max 2550PC, Japan). Scanning electron microscopy (SEM, JSM-6700F, USA) was used to observe the fiber morphology of DA/PVDF nanofiber membranes. The water contact angle (WCA) of all samples was measured with Data Physics (OCA20, German).

Electrical Output Measurements

The PVDF and DA/PVDF nanofiber membranes were cut to the desired dimensions of 2.0×2.0 cm^2. The membranes were sandwiched with a pair of electrodes, and then wrapped in polyimide tap. To measure the output produced by the membranes under LIPUS stimulation, the device was placed under a LIPUS probe. LIPUS was generated using a digital ultrasound device (Sonicator 740, Mettler Electronics, USA) with a probe diameter of 35 mm, a frequency of 1 MHz, and a pulse duration of 1.4 ms. The applied power intensities were ranged from 0.0 W/cm^2 to 1.0 W/cm^2 (ie, 0.2 W/cm^2, 0.4 W/cm^2, 0.6 W/cm^2, 0.8 W/cm^2, and 1.0 W/cm^2). The electric outputs (voltages) generated from the membranes were obtained using a potentiostat (CHI660E, China). Furthermore, alterations in the real-time electrical signals of DA/PVDF nanofiber membranes that applied to mouse dorsal skin wounds (defect of 1 square centimeter wound in the center of the mouse back), in response to LIPUS intervention were quantified through measurements with the PowerLab 26T (ADInstruments, AU).

Cell Attachment and Morphology

L929 cells were inoculated onto PVDF and DA/PVDF nanofiber membranes, followed by stimulation with LIPUS. After 24 hours, the morphology of the cells on the membrane surfaces was examined using scanning electron microscopy (SEM; JSM-6700F, USA) and fluorescence microscopy (DP74, OLYMPUS, China). In this study, different membranes of 2 mm diameter were added to each well of a 12-well plate at a cell density of 5×10^4 cells per well. After 24 hours of culture in complete medium, the membranes were fixed in 4% paraformaldehyde for 30 minutes at 37°C. After three washes with PBS, the cytoskeleton was stained with rhodamine (Solabio, China) for 30 min and 4',6-diamino-2-phenylindole (Solabio, China) for 5 min at 37°C. Finally, after three washes with PBS to remove the stain, the morphology of the cells on the membrane surfaces was examined using fluorescence microscopy (DP74, OLYMPUS, China) and scanning electron microscopy (SEM; JSM-6700F, USA). Furthermore, to assess the adhesion of the membranes to cells at wound sites in mice under LIPUS stimulation (1.0 W/cm^2, 5 min), PVDF and DA/PVDF nanofiber membranes (1.0 × 1.0 cm^2) were implanted into the dorsal skin. Following a 24-hour incubation period, the samples were retrieved and subjected to SEM imaging.

Evaluation of Cell Viability on DA/PVDF Nanofiber Membranes by CCK8 Assay

Using 12-well polystyrene plates (TCPs), the L929 fibroblast cell line was inoculated on PVDF or DA/PVDF nanofiber membranes and cells cultured on bare TCPs were used as a control (5×10^4 cells per well). After inoculation, the cells were incubated in Dulbecco's Modified Eagle's Medium (DMEM) with 10% fetal bovine serum (FBS) and 1% penicillin-streptomycin (P-S, Gibco) at 37°C for 24 h, 48 h, and 72 h. In this experiment, the LIPUS ultrasound probe was attached to the bottom of the culture plate and an ultrasound gel coating was applied between the probe and the culture plate. The objective was to facilitate the penetration of ultrasound into the TCPs, thereby inducing deformation of

nanofiber membranes and generating electrical stimulation. The parameters of LIPUS ultrasound stimulation were set as follows: 5 min per day, using different power intensities (ie, 0.2 W/cm^2, 0.4 W/cm^2, 0.6 W/cm^2, 0.8 W/cm^2, 1.0 W/cm^2). The LIPUS frequency was 1 MHz and the pulse duration was 1.4 ms. At 24 h, 48 h, and 72 h time points, the medium was aspirated and replaced with 500 μL of fresh medium and 50 μL of Cell Counting Kit-8 (CCK-8) (NCM Biotech, China) solution, and incubated for 2 h at 37°C. Finally, the solution was transferred to a 96-well plate (100 μL per well) and the absorbance value at 450 nm was determined using an enzyme labeler (SynergyHT, BioTek, USA). The relative cell viability was calculated as follows:

$$Cellviabillity\,(\%) = \frac{At - Ab}{Ac - Ab} \times 100$$

In this experiment, *At* represents the absorbance of experimental groups, *Ab* represents the absorbance of blank groups, and *Ac* represents the absorbance of control groups.

Trans-Well Assay

Fibroblast migration was assessed by the scratch assay. L929 cells were inoculated at a density of 5×10^4 cells per well (500 μL/well, 24-well TCP) in low-nutrient medium (1% fetal bovine serum in DMEM) incubated overnight at 37°C. After cell attachment, the cell layer was scratched with a pipette tip. Then, a circular PVDF nanofiber mat (diameter: ~ 1 cm) was immersed into the supernatant and the nanofiber membranes were vibrated using LIPUS (1 MHz, 0.2–1.0 W/cm^2, 1.4 ms pulse duration).

In order to gain further insight into the effects of PVDF and DA/PVDF nanofiber membranes on cell migration, The trans-well method was employed under LIPUS ultrasound at 1.0 W/cm^2. Cells were inoculated into the upper chamber of a 12-well Trans-well plate (pore size: 8) and starved of serum in 500 μL serum-free medium for 24 h. PVDF nanofiber membranes and DA/PVDF nanofiber membranes were placed at the bottom of the lower chamber, and the bottom of the plate was coated with gel to facilitate ultrasound penetration. After 5 minutes of LIPUS stimulation, the plates were incubated for 24 h at 37°C and 5% carbon dioxide. After 24 hours, the upper chamber was removed, and the top cells were gently wiped away with a cotton swab. The cells were fixed with 4% paraformaldehyde at 37°C for 30 min and washed three times with PBS. Finally, the cells were stained with 5% crystal violet solution.

In vivo Animals Test

Six-week-old female ICR mice (20 g) were used for wound healing experiments. Seventy-five ICR mice were randomly divided into 5 groups: the blank control group, the fibrin glue group, the LIPUS group, the DA/PVDF groups and the DA/PVDF+LIPUS group (n = 15). Mice were anesthetized with 4% w/v chloral hydrate (0.1 mL/10g) and then the dorsal hair of each mouse was removed using an electric razor, and 1.0 cm × 1.0 cm square full-thickness skin defects were made on the backs of the mice after they were cleaned with 75% alcohol for each mouse. All animal procedures were performed in accordance with the Guidelines for Care and Use of Laboratory Animals of Changchun Institute of Applied Chemistry Chinese Academy of Sciences and approved by Institutional Animal Care and Use Committee of Changchun Institute of Applied Chemistry Chinese Academy of Sciences (Permit Number: 20210016). The blank control, commercial control and experimental groups were washed with saline, 0 wrapped in gauze and secured with 3M tape. In the LIPUS group and DA/PVDF+LIPUS group, LIPUS treatment was administered once a day at a power intensity of 1.0 W/cm^2 for a total of 5 minutes. Digital photographs of the wounds at different time points were obtained and the size of the wounds at different days (0, 3, 7, and 14) was measured using Image J software. The relative wound healing area was calculated:

$$\text{Relative wound healing area}\,(\%) = \frac{\text{At}}{\text{A0}} \times 100$$

where A0 and At are the wound areas of 0 d and x d (x = 3, 7 and 14) after treatment, respectively.

On days 3, 7 and 14 following treatment, histopathological analysis was conducted on the skin tissue surrounding the wound of the different groups. Furthermore, histopathological analysis was conducted on the major organs, including the heart, liver, spleen, lungs, and kidneys, on the 14th day post treatment. Tissue samples were collected and fixed in 4%

formaldehyde. The tissues were subjected to hematoxylin and eosin (H&E) or Masson trichrome staining, after which the sections were observed under a microscope (DP73, Olympus, Tokyo, Japan).

Statistical Analysis

Quantitative data were expressed as mean ± standard deviation (SD). One-way analysis of variance (ANOVA) was performed using GraphPad Prism software to analyze the statistical differences between the control and treatment groups, and p-values less than 0.05 were considered statistically significant in the analysis (*$P < 0.05$, **$P < 0.01$, ***$P < 0.001$, ****$P < 0.0001$).

Results and Discussion

Preparation and characterization of the DA/PVDF Nanofiber Membrane

DA/PVDF nanofiber membranes were prepared by the electrospinning method as shown in Scheme 1. Scanning electron microscopy (SEM) images illustrated morphological differences between PVDF nanofiber membranes before and after incorporating DA molecules (1.0 wt%) (Figure 1a). The fiber diameters ranged from nanometers to micrometers, with the dimensional span increasing upon the addition of DA molecules. After incorporating DA, the diameter distribution of the DA/PVDF nanofibers was approximately 732 ± 232 nm, compared to 712.34 ± 163.42 nm for pristine PVDF nanofibers

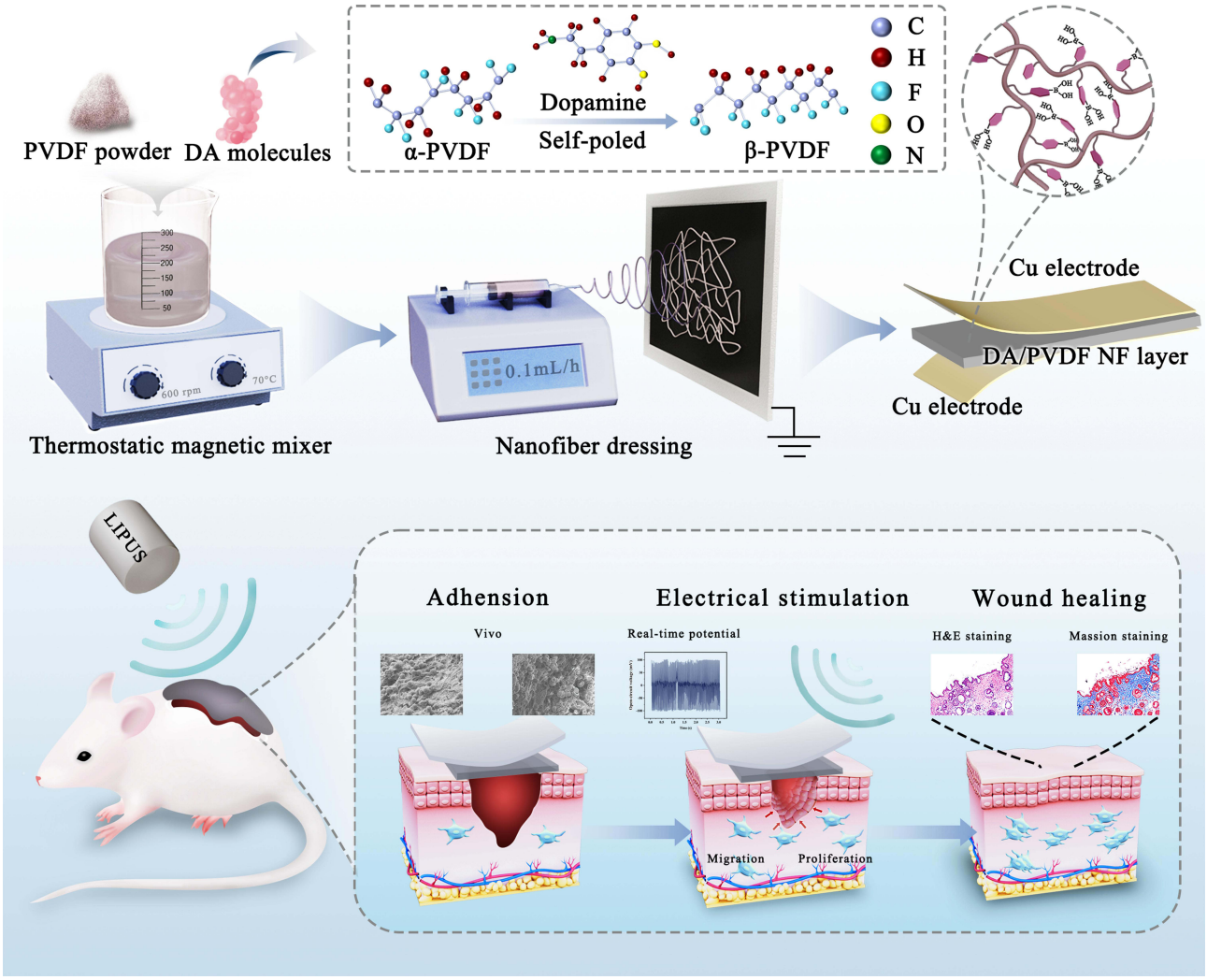

Scheme 1 Schematic diagram of the fabrication and application of PVDF nanofiber membrane and DA/PVDF nanofiber membrane.

(Figure 1b). Notably, the DA/PVDF nanofiber membranes exhibited a higher proportion of small-diameter fibers. This increase in small fibers may be attributed to enhanced electrostatic repulsion induced by dopamine, which produces a "twitching effect" during the electrospinning process, leading to the formation of small nanofibers.[23,24] Additionally, transmission electron microscopy (TEM) images revealed distinct phase separation within DA/PVDF nanofibers and provided evidence of a "twitching effect" occurring during the electrospinning process (Figure S1).

The chemical structures of the nanofibers were further analyzed using FTIR and XRD spectroscopy (Figure 1c and d). As shown in Figure 1c, both PVDF and DA/PVDF nanofiber membranes exhibit a distinct peak at 840 cm^{-1}, corresponding to the polar β-phase. Notably, the 1.0 wt% DA/PVDF nanofiber membranes exhibited the most pronounced characteristic peak. In contrast, the characteristic peaks associated with the nonpolar α-phase (eg, 763 cm^{-1} and 796 cm^{-1}) were not prominently observed in either nanofiber membrane, which might due to the structural modifications induced by the electrospinning process.[25,26] During the electrospinning process, the high-voltage electric field induces polarization of PVDF, promoting the formation of the polarized β-phase. XRD measurements were performed in the 10° - 40° range at an angle of 2θ as shown in Figure 1d. The absence of the characteristic α-phase peak at 26.6° (021) in both PVDF and DA/PVDF nanofibers may be also attributed to the high-voltage electric field applied during the electrospinning process. At 20.6°, there is a more prominent characteristic peak of β-phase in DA/PVDF compared to PVDF (110/200), which suggests that the β-phase of DA/PVDF is more crystalline. Moreover, in comparison to PVDF, DA/PVDF exhibits a weaker shoulder peak at 18.6° (202), which provides further evidence of a higher degree of transition from the α-phase to the β-phase and a lower degree of excess of the γ-phase in DA/PVDF. DA can act as a nucleating agent and promote PVDF crystallization, thereby leading to an increase in the formation of the piezoelectric β-phase.

As shown in Figure 1e and f, the hydrophilicity of PVDF nanofiber membranes were significantly enhanced following DA modification, as evidenced by a reduction in the contact angle from 138.2 ± 1.3° to 88.4 ± 1.9°. This increased hydrophilicity will promote cell anchoring, adhesion, and stretching, which may also facilitate the deformation of the electrospun film due to enhanced cellular stress stretching. This, in turn, could stimulate the generation of electrical currents. Furthermore, the yield strength of the DA/PVDF nanofiber membranes improved compared to the PVDF nanofiber membranes (Figure 1g), indicating the recovery of toughness in the DA/PVDF nanofiber membranes. The yield strength and toughness of the material are closely related to its piezoelectric properties. Higher mechanical strength and toughness means that DA/PVDF is able to generate electrical signals more consistently under mechanical stresses.[27] Additionally, Higher yield strength and toughness can provide a stable mechanical microenvironment for cells, which contributes to cell attachment and functionalization.[28]

Electric Outputs of the DA/PVDF Nanofiber Membranes Under LIPUS Stimulation

The electrical output of DA/PVDF piezoelectric membranes driven by Low-Intensity Pulsed Ultrasound (LIPUS) was investigated across a range of power intensities from 0.0 to 1.0 W/cm^2. As shown in Figure 2a, PVDF nanofiber membranes produced a maximum output voltage of approximately 350 mV in response to LIPUS stimulation at 1.0 W/cm^2 with a pulse duration of 1.4 ms. Upon the addition of 1.0% DA, a notable increase in the maximum voltage output of the DA/PVDF nanofiber membranes were observed under identical LIPUS conditions, reaching approximately 450 mV. This represents a 1.28-fold enhancement compared to the PVDF nanofiber membranes alone, indicating that DA significantly augments the piezoelectric response of the membranes to ultrasonic stimulation. The local electrical output of DA/PVDF nanofiber membranes placed on mouse skin under LIPUS stimulation at 1.0 W/cm^2 was further investigated. Under LIPUS stimulation (1.0 W/cm^2, 1 MHz), the piezoelectric nanofiber membranes exhibited localized real-time voltages averaging 45.90 ± 36.20 (Figure 2b and Video S3). The results indicate that DA/PVDF piezoelectric membranes have the potential to create a microenvironment with an electrical potential comparable to a transepithelial potential (TEP) of the skin (10–60 mV),[29] and thus show promise for restoring electrical signals at wound sites under ultrasound stimulation. Furthermore, the influence of varying LIPUS intensities on the output characteristics of DA/PVDF piezoelectric membranes in vitro was also investigated (Figure 2c). The results also revealed a significant increase in the electrical output of the piezoelectric membranes as LIPUS power intensity increased from 0.0 to 1.0 W/cm^2. In conclusion, these results demonstrate that DA-modified PVDF piezoelectric membranes exhibit significantly enhanced

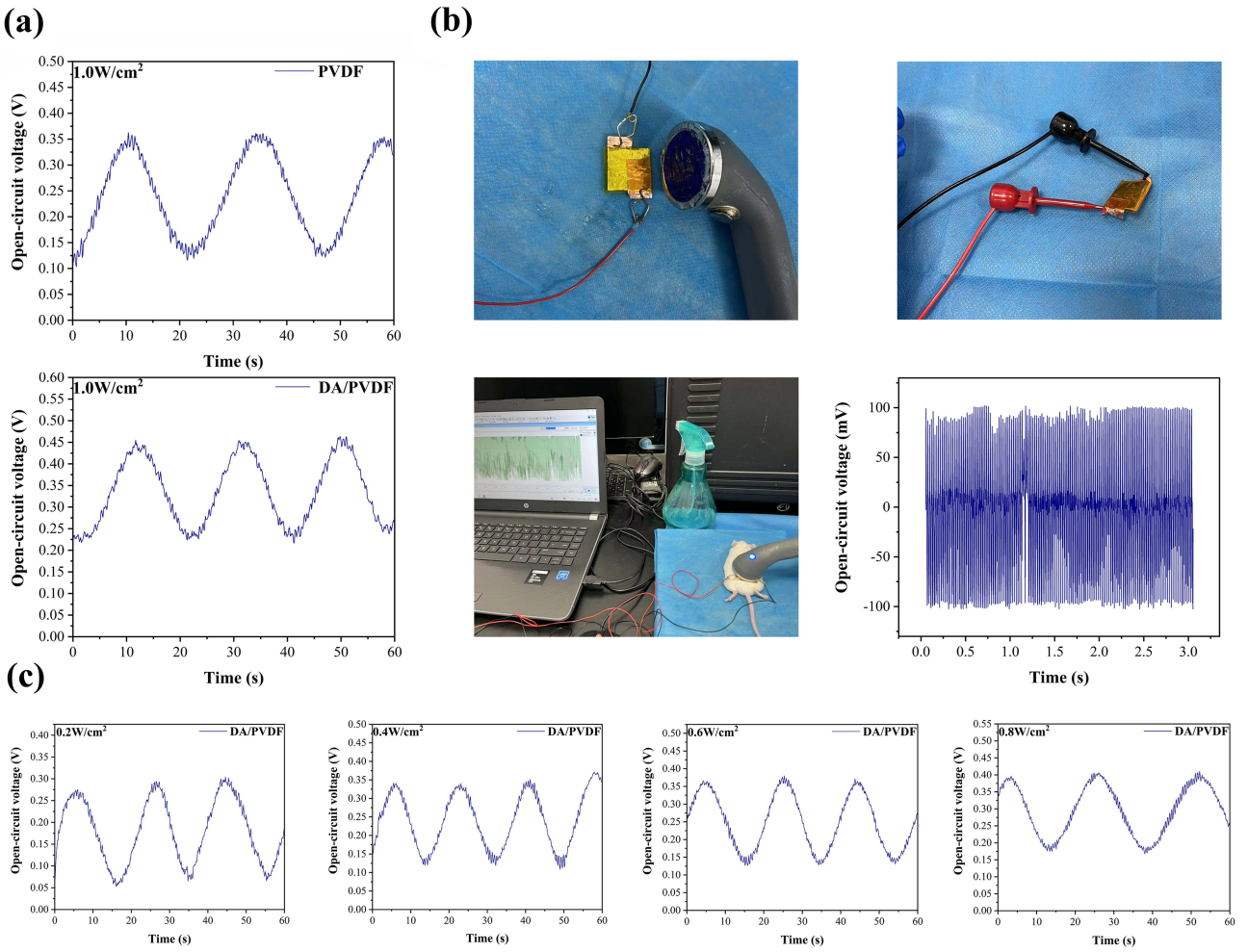

Figure 2 Electrical output properties of DA/PVDF membranes under LIPUS stimulation. (**a**) The output voltage generated by the PVDF piezoelectric membrane and the DA/PVDF piezoelectric membrane in response to LIPUS stimulation at a power density of 1.0 W/cm^2. (**b**) The output voltage generated by the DA/PVDF membrane, activated by LIPUS ultrasound. (**c**) The output voltage of the DA/PVDF piezoelectric membrane under LIPUS ultrasonic stimulation with varying power intensities.

piezoelectric properties in response to LIPUS stimulation, suggesting its potential utility in activating piezoelectric properties of electrospun nanofiber membranes for restoring electrophysiology of skin wound.

Cell Adhesion on DA/PVDF Nanofiber Membranes Both in vitro and in vivo Under LIPUS

The adhesive properties of wound dressings play a critical role in wound management, as they facilitate the maintenance of a moist microenvironment, which is essential for optimal cell proliferation, enhanced collagen synthesis, and efficient tissue repair.[30,31] In order to detect cell adhesion features, PVDF and DA/PVDF nanofiber membranes were prepared into circular samples as shown in Figure 3a. The original PVDF nanofiber membranes were shown white in color and tended to be brownish-yellow in color after dopamine modification. After 24 hours of culture, laser confocal imaging of L929 cells on PVDF and DA/PVDF nanofiber membranes, with or without LIPUS (1.0 W/cm²) stimulation, revealed that DA/PVDF membranes significantly enhanced cell adhesion, which was further improved by LIPUS stimulation (Figure 3b). In contrast, the PVDF nanofiber membranes had much less cells adhesion, which is attribute to the superhydrophobic PVDF. The results demonstrated that DA-modification significantly enhance the hydrophilicity and thus promote cell adhesion. In addition, the results also indicated that LIPUS could promote cell adhesion, which may due the activation of fibronectin-dependent signaling.[32] In addition, SEM images of the morphology of L929 cells on these nanofiber membranes under similar conditions were shown in Figure 3c, highlighting extensive cell adhesion and an elongated, stretched morphology forming a continuous cell layer, particularly on DA/PVDF nanofiber membranes with LIPUS.

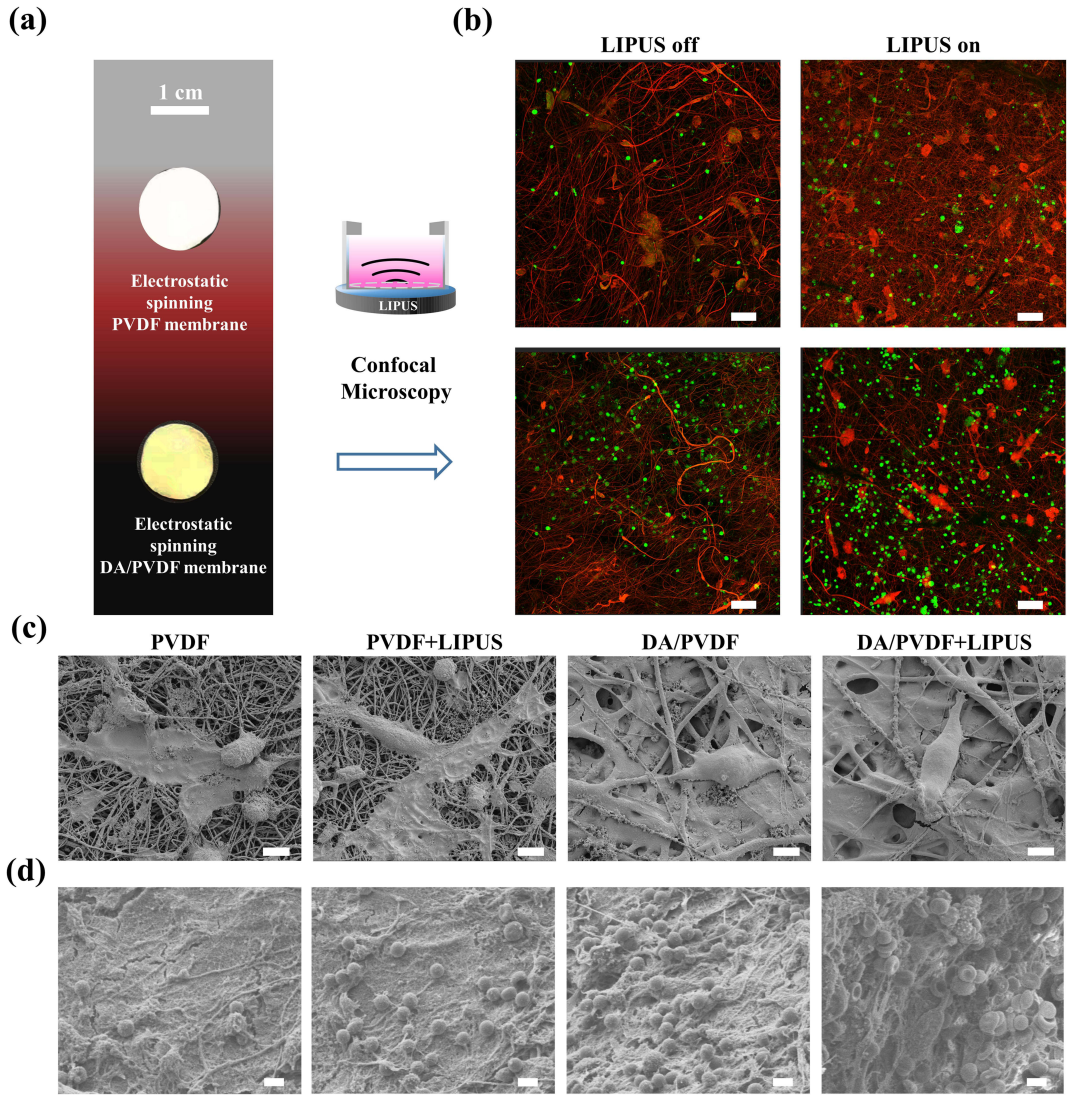

Figure 3 Cell adhesion to electrospun PVDF nanofiber membranes and DA/PVDF nanofiber membranes. (**a**) Physical drawings of electrospun PVDF nanofiber membrane and electrospun DA/PVDF nanofiber membrane. (**b**) Laser confocal images of L929 cells inoculated on PVDF nanofiber membranes and DA/PVDF nanofiber membranes and cultured for 24 hours after LIPUS stimulation with and without 1.0 W/cm^2 (scale bar = 100 μm). (**c**) SEM images of L929 cells inoculated on PVDF nanofiber membranes and DA/PVDF nanofiber membranes and cultured for 24 h after LIPUS stimulation with and without 1.0 W/cm^2 (scale bar = 10 μm). (**d**) SEM images of PVDF and DA/PVDF piezoelectric membranes immobilized on the dorsal skin of mice after 24 hours of stimulation without and with LIPUS (1.0 W/cm^2) (scale bar = 4 μm).

These findings demonstrate that both dopamine modification and LIPUS stimulation significantly enhance cell adhesion on PVDF nanofiber membranes, exhibiting a superimposed effect.

To verify the real situation of cells adhesion on DA/PVDF nanofiber membranes under LIPUS stimulation at the wound site, the PVDF nanofiber membranes and DA/PVDF nanofiber membranes were applied to mouse dorsal skin wounds (defect of 1 square centimeter wound in the center of the mouse back), and the nanofiber membranes were stimulated using LIPUS (1.0 W/cm^2, 5 min/24h). After 24 hours, the collected nanofiber membranes were evaluated by SEM, the results showed significant blood cell aggregation on the DA/PVDF nanofiber membranes, especially in the LIPUS-stimulated group, indicating enhanced cell recruitment (Figure 3d). Particularly, this effect will promote clot formation which could contributes to the initiation of damage repair.[33] Thus, DA modification of PVDF nanofiber membranes greatly improved cell adhesion, promoted clot formation, benefits further augmented by LIPUS stimulation, making this combination promising for wound healing applications.

https://doi.org/10.2147/IJN.S496921

DA/PVDF Nanofiber Membranes Promotes Cell Proliferation and Migration Under LIPUS

Herein, we investigated the effects of various ultrasound parameters on cell proliferation of L929 fibroblasts inoculated onto DA/PVDF nanofiber membrane in 24-well plates for 3 consecutive days using the CCK-8 assay.[34] After 1 day of incubation, there was no significant difference in the proliferative activity of the groups of cells between LIPUS-treated and untreated groups as shown in Figure S2. In contrast, after 2 days of incubation, the proliferation of cells on DA/PVDF showed an increase under LIPUS compared to PVDF groups as shown in Figure S3. Notably, the TCP control groups (tissue culture polystyrene) displayed higher proliferative activity than PVDF alone. This implied that the significantly increased hydrophilic character after modification of DA was critical for cell proliferation. As illustrated in Figure 4a, after 3 days of incubation, cell viability on both PVDF nanofiber membranes and DA/PVDF nanofiber membranes without LIPUS (0 W/cm^2) was higher compared to the control group. Notably, the DA/PVDF group showed significantly enhanced cell viability compared to the PVDF nanofiber membranes and TCP groups. Upon adjusting the LIPUS power to 0.2 W/cm^2, 0.6 W/cm^2, and 0.8 W/cm^2, the cell viability on the DA/PVDF nanofiber membranes increased relative to the TCPs control group. Overall, the DA/PVDF nanofiber membranes plus LIPUS stimulation showed an increased effects on cell proliferation compared to other groups, particularly under high power sonication (1.0 W/cm^2). As shown in Figure 4b, after 3 days of incubation, when the LIPUS power intensity was adjusted to 1.0 W/cm^2, the cell viability on the DA/PVDF nanofiber membrane was 1.14 times higher than that of the TCP control groups ($P < 0.001$). These results showed that the DA/PVDF piezoelectric nanofiber membranes plus LIPUS stimulation can efficiently generate electrical stimulation on fibroblasts and promoting cell proliferation.

In addition, transwell experiments were performed to investigate cell migration behavior under LIPUS stimulation.[35,36] The results further revealed the combinatorial benefits of DA/PVDF and LIPUS (Figure 4c and d). Under 1.0 W/cm² LIPUS, DA/PVDF membranes facilitated 244.67 ± 7.85 migrated cells/field, significantly surpassing both PVDF (198.33 ± 6.94, **P<0.01) and TCP controls (198.33 ± 14.72, **P<0.01). In addition, even without LIPUS, DA/PVDF promoted migration (214.33 ± 13.81 vs 177 ± 9.90 for PVDF, P<0.05), potentially attributable to DA-mediated integrin activation via surface-bound catechol motifs.[37] Collectively, our results indicate that the combination of DA/PVDF nanofiber membranes with LIPUS synergistically enhances fibroblast proliferation and migration via dual

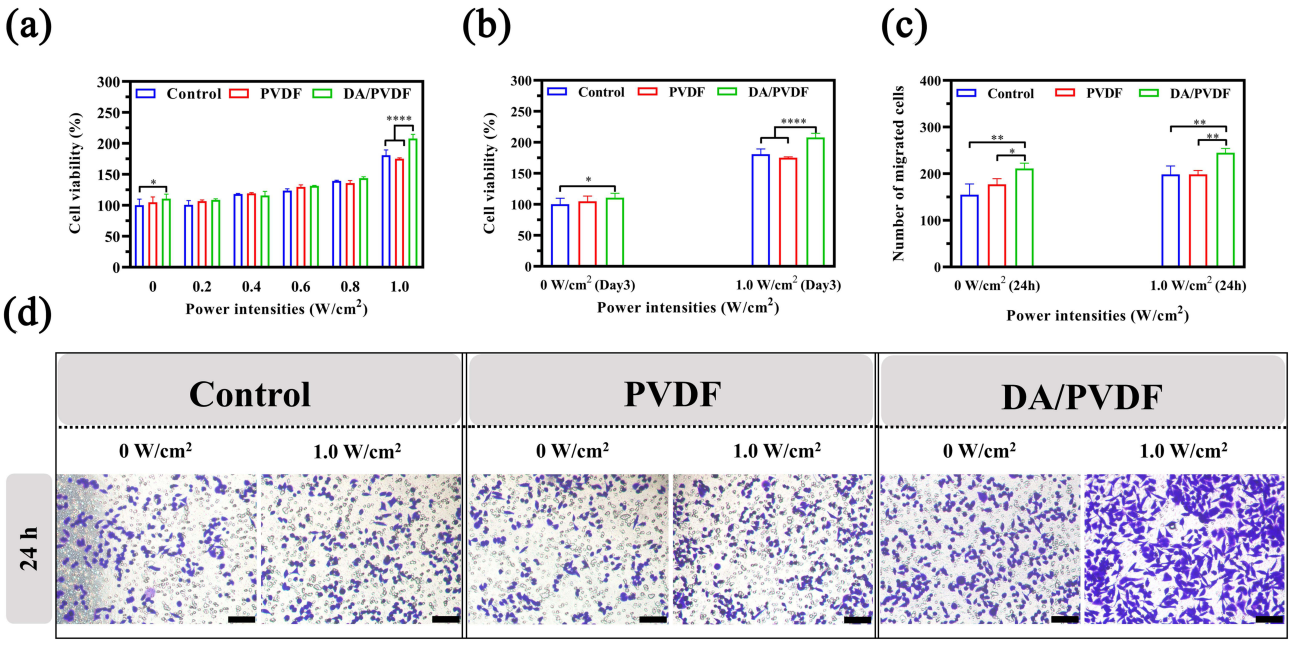

Figure 4 L929 fibroblast viability and migration on piezoelectric membranes under LIPUS stimulation. (**a**) Cell viability percentages measured by the CCK-8 assay across different groups and power intensities. (**b**) Cell viability on day 3 for PVDF and DA/PVDF membranes under 0 W/cm² and 1.0 W/cm² power intensities. (**c**) Quantitative analysis of transwell experiments. (**d**) Microscopic images showing cell migration at 24 hours under different power intensities and treatment conditions. (n = 3, scale bar = 500 μm). Asterisks indicated statistically significant differences (*$P < 0.05$, **$P < 0.01$, ****$P < 0.0001$).

mechanisms. These include piezoelectric-driven electrical stimulation under ultrasound exposure and DA-induced enhancements in hydrophilicity and biochemical signaling.

In vivo Wound Healing Behaviors of DA/PVDF Under LIPUS

The classification of skin defects is dependent on the depth of injury. These defects can be categorized as epidermal skin wounds, superficial partial-thickness skin wounds, deep partial-thickness skin wounds, and full-thickness skin wounds.[38] In order to investigate the potential efficacy of the DA/PVDF under the stimulation of LIPUS (1.0 W/cm^2) in promoting wound healing, we conducted repair tests on full-thickness skin defects in mice. Full-thickness skin wounds (1 × 1 cm^2) were created on the dorsal skin of each mouse. The experimental groups were designated as follows: Control, Fibrin, LIPUS, DA/PVDF, and DA/PVDF + LIPUS groups. The control group consisted of mice in which the full-thickness skin wounds were not treated. The specific treatment protocol is depicted schematically in Figure 5a. On days 0, 3, 7 and 14 the wound healing process was observed and recorded using a camera. The representative image, depicted in Figure 5b, presents the results of this data set, which has been subjected to a wound contraction simulation (Figure 5d). By the third day, all experimental groups displayed an absence of visible erythema and edema, alongside a notable extension and proliferation of epidermal tissue into the central region of the wound. By day 14, wounds treated with DA/PVDF + LIPUS had largely healed, in contrast to the other groups

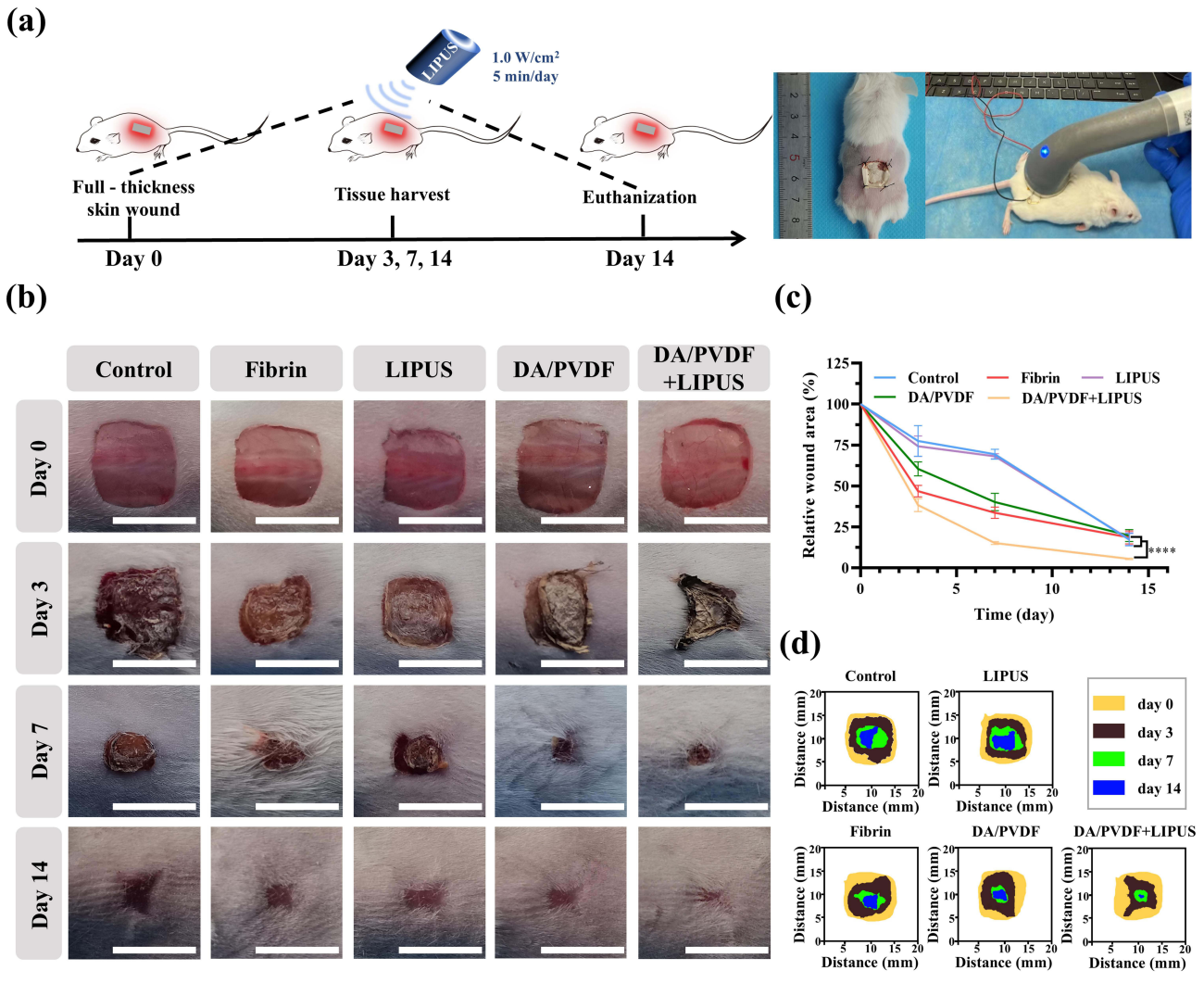

Figure 5 Repair of full-thickness skin wounds in mice by LIPUS responsive piezoelectric DA/PVDF nanofiber membranes. (**a**) Schematic diagram of creating full-thickness skin wounds in mice and applying LIPUS stimulation. (**b**) Photographs of the wounds exposed to different treatments (scale bar = 1 cm). (**c**) Quantitative analyzation of the remaining area of skin defects. (**d**) Corresponding wound marks. Asterisks indicated statistically significant differences (****$P < 0.0001$).

https://doi.org/10.2147/IJN.S496921

where significant residual wound areas remained. Furthermore, the DA/PVDF + LIPUS group exhibited no visible scarring at the wound site, in stark contrast to the observable scarring present in the other experimental cohorts. To further evaluate the rate of wound healing, the remaining area of skin defects were quantitatively analyzed. As shown in Figure 5c, the defective area of each group decreased with time. On day 3, the wound healing rates of the Control group, Fibrin group, LIPUS, DA/PVDF group, and DA/PVDF+LIPUS group treatments were 23%, 39%, 50%, 60%, and 68%, respectively. The wound healing rate of the DA/PVDF+LIPUS group treatments reached 85% on day 7, which was significantly higher than that of the other groups. After 14 days of treatment, the visible wounds defects were still evident and covered by scabs in the Control group, Fibrin group, LIPUS group, and DA/PVDF group (healing rate is less than 80%), whereas the wounds in the DA/PVDF +LIPUS group were almost completely closed (healing rate is more than 95%). In addition, there was no visible scarring or elevation in the DA/PVDF+LIPUS group, and the color of the newly regenerated skin was similar to that of the adjacent normal tissue (Figure 5c). By analyzing the quantitative wound healing data (Figure 5b) and the trauma trajectories (Figure 5d), it can be seen that DA/PVDF + LIPUS is more effective in promoting wound healing compared to the other groups. These results suggest that the utilization of LIPUS (1.0 W/cm^2) responsive DA/PVDF piezoelectric films on wounds could significantly expedite the healing process.

To histological evaluate the reconstruction of the tissue in the wound, skin samples were collected on days 3, 7, and 14. Then, they were subjected to histological examination, using both H&E and Masson trichrome staining. Epidermal defects were observed on day 3, and all wounds exhibited mild acute inflammation, with macrophages and fibroblasts accumulating at the wound site. It is noteworthy that the inflammatory cell infiltration was markedly reduced in the DA/PVDF+LIPUS group (Figure S4). On day 7, the wound site treated in DA/PVDF group, DA/PVDF +LIPUS group had a complete epidermis, which was not observed in the blank group, commercial dressing group, and LIPUS group (Figure S5). On day 14, complete epidermal tissue is formed and granulation tissue disappears in all groups (Figure 6a). Figure 6c shows the quantitative analysis of wound length on day 14. A statistically significant difference was observed between the DA/PVDF+LIPUS group and the blank group, with wound healing lengths of 0.25 ± 0.09 mm and 3.61 ± 0.37 mm, respectively. More importantly, the number of follicular structures (27.33 ± 4.5) and blood vessels (27.33 ± 5.1) formed in the DA/PVDF+LIPUS group was superior to the other groups, demonstrating the regeneration of normally functioning skin tissue (Figure 6d and e).

During the remodeling phase of wound healing, type III collagen fibers are initially deposited and then remodeled to type I.[39] Masson trichrome staining showed that the control group had fewer collagen fibers in the early stage of wound healing (Figure S6). It is noteworthy that in the later stages of wound healing (14 days), as collagen fibers deposition increased, the collagen fibers in the DA/PVDF+LIPUS group exhibited a more ordered and regular arrangement, in contrast to the irregular spiral shape observed in the control group (Figure 6b and Figure S7). A notable phenomenon was observed during an in-depth investigation into the wound healing effects of DA/PVDF+LIPUS composites. The treatment group demonstrated a trend of reduced of type I collagen deposition at the wound site, with a value of 37.20 ± 2.80 (Figure 6f). This finding is closely related to the intrinsic dynamics of wound healing. The synthesis and deposition of collagen fibers normally increases dramatically in the early stages of the process, a process that is essential to support and stabilize the newly formed tissue.[40] However, during the remodeling phase, as the wound heals into the subsequent stages of the healing process, the synthesis and degradation of collagen is gradually balanced to prevent unwanted scarring due to excessive collagen deposition.[41] It can be posited that the DA/PVDF+LIPUS group commenced the remodeling phase of wound healing at an earlier stage than the control group and the other experimental groups. In addition, H&E staining of the major organs of the mice in the figure showed no significant difference between the groups, indicating that all treated strategies had no apparent toxicity (Figure S8). In conclusion, the above results demonstrate that DA/PVDF +LIPUS can promote re-epithelialization of skin wounds in mice, promote collagen formation and remodeling, as well as promote vascular and dermal appendage regeneration. LIPUS responsive DA/PVDF offer a new promising strategy for full-thickness skin wound healing.

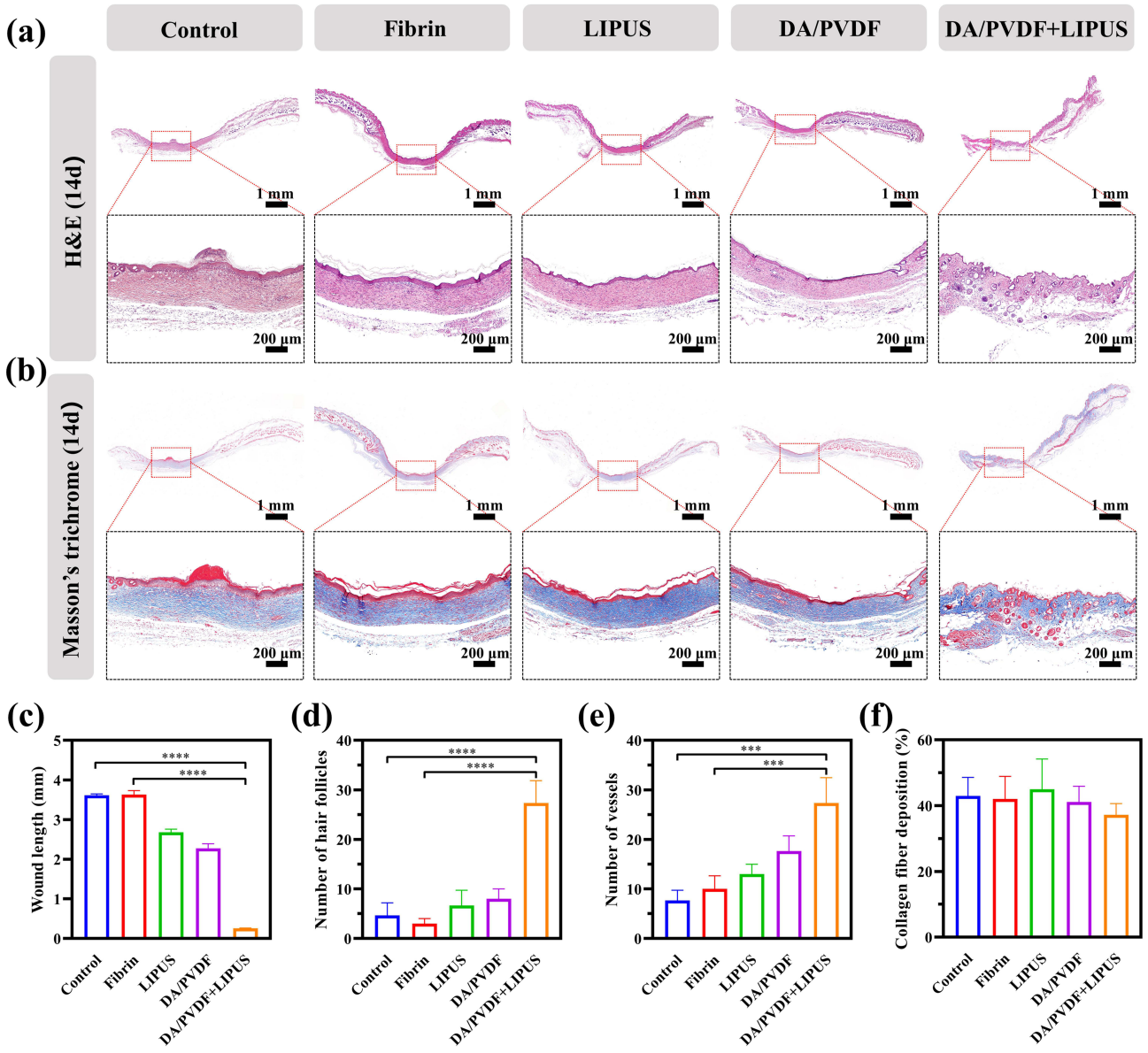

Figure 6 Histological analysis of wound healing at 14 days. (**a**) H&E staining of skin wounds tissue after treatment. (**b**) Masson trichrome stain images of skin wound tissue after treatment. The second row is an enlarged image of the dotted box in the first row. (**c**) Quantification of size of the defect area in each group. (**d**) The number of new hair follicles that are formed in the repaired skin defects. (**e**) The number of new vessels that are formed in the repaired skin defects. (**f**) Statistical quantification of collagen in Masson trichrome stained images analyzed using ImageJ. Asterisks indicated statistically significant differences (***$P < 0.001$, ****$P < 0.0001$).

Conclusion

This study presents a novel strategy to enhance wound healing using dopamine-modified polyvinylidene fluoride (DA/PVDF) nanofiber membranes combined with Low-Intensity Pulsed Ultrasound (LIPUS) stimulation. The DA modification promoted the formation of the piezoelectric β-phase in PVDF, enhancing its piezoelectric properties and electrical output under LIPUS. These properties, combined with LIPUS, significantly improved cell adhesion, proliferation, and migration in vitro. In vivo experiments on full-thickness skin defects in mice demonstrated that the DA/PVDF nanofiber membranes, coupled with LIPUS, accelerated wound healing, improved tissue reconstruction, and enabled scar-free healing with skin appendage regeneration. This approach offers a promising strategy for regenerating fully functional skin tissue. Further studies are needed to understand the mechanism of piezoelectric-induced regeneration of skin appendages.

https://doi.org/10.2147/IJN.S496921

Funding

This study was financially supported by the Science and Technology Project of Jilin Provincial Department of Finance (JCSZ 2020304-21) and Industrialization Cultivation Project of Jilin Provincial Education Department (JJKH20201114KJ).

Disclosure

The authors declare no conflict of interest.

References

1. Barros Almeida I, Garcez Barretto Teixeira L, Oliveira de Carvalho F, et al. Smart dressings for wound healing: a review. *Adv Skin Wound Care*. 2021;34(2):1–8. doi:10.1097/01.ASW.0000725188.95109.68
2. Markiewicz-Gospodarek A, Kozioł M, Tobiasz M, et al. Burn wound healing: clinical complications, medical care, treatment, and dressing types: the current state of knowledge for clinical practice. *Int J Environ Res Public Health*. 2022;19(3):1338. doi:10.3390/ijerph19031338
3. Zhang Y, Demir B, Bertsch G, et al. Zwitterion and N-halamine functionalized cotton wound dressing with enhanced antifouling, antibacterial, and hemostatic properties. *Int J Biological Macromol*. 2023;230:123121. doi:10.1016/j.ijbiomac.2022.123121
4. Huang H, Chen L, Hou Y, et al. Self-assembly of chlorogenic acid into hydrogel for accelerating wound healing. *Colloids Surf B Biointerfaces*. 2023;228:113440. doi:10.1016/j.colsurfb.2023.113440
5. Ding Y, Sun Z, Shi R, et al. Integrated endotoxin adsorption and antibacterial properties of cationic polyurethane foams for wound healing. *ACS Appl Mater Interfaces*. 2019;11(3):2860–2869. doi:10.1021/acsami.8b19746
6. Dai J, Shao J, Zhang Y, et al. Piezoelectric dressings for advanced wound healing. *J Mater Chem B*. 2024;12(8):1973–1990. doi:10.1039/d3tb02492j
7. Kim HS, Sun X, Lee JH, et al. Advanced drug delivery systems and artificial skin grafts for skin wound healing. *Adv Drug Deliv Rev*. 2019;146:209–239. doi:10.1016/j.addr.2018.12.014
8. Xu X, Zhang H, Yan Y, et al. Effects of electrical stimulation on skin surface. *Acta Mech Sin*. 2021;37(12):1843–1871. doi:10.1007/s10409-020-01026-2
9. Luo R, Dai J, Zhang J, et al. Accelerated skin wound healing by electrical stimulation. *Adv Healthc Mater*. 2021;10(16):e2100557. doi:10.1002/adhm.202100557
10. Swain S, Misra RDK, Rautray TR. Nanoscale generators for tissue healing: a perspective. *Int J Nanomed*. 2024;19:11859–11882. doi:10.2147/IJN.S480938
11. Andrey V, Koshevaya E, Mstislav M, et al. Piezoelectric PVDF and its copolymers in biomedicine: innovations and applications. *Biomater sci*. 2024;12(20):5164–5185. doi:10.2147/ijn.S480938
12. Du S, Zhou NY, Gao YJ, et al. Bioinspired hybrid patches with self-adhesive hydrogel and piezoelectric nanogenerator for promoting skin wound healing. *Nano Res*. 2020;13(9):2525–2533. doi:10.1007/s12274-020-2891-9
13. Fu RM, Tu LJ, Zhou Y, et al. A tough and self-powered hydrogel for artificial skin. *Chem Mat*. 2019;31(23):9850–9860. doi:10.1021/acs.chemmater.9b04041
14. Qiu WZ, Yang HC, Xu ZK. Dopamine-assisted co-deposition: an emerging and promising strategy for surface modification. *Adv Colloid Interface Sci*. 2018;256:111–125. doi:10.1016/j.cis.2018.04.011
15. Ho CC, Ding SJ. Structure, properties and applications of mussel-inspired polydopamine. *J Biomed Nanotechnol*. 2014;10(10):3063–3084. doi:10.1166/jbn.2014.1888
16. Li B, Xiong F, Yao B, et al. Preparation and characterization of antibacterial dopamine-functionalized reduced graphene oxide/PLLA composite nanofibers. *RSC Adv*. 2020;10(32):18614–18623. doi:10.1039/d0ra03224g
17. Li T, Jin F, Qu M, et al. Power generation from moisture fluctuations using polyvinyl alcohol-wrapped dopamine/polyvinylidene difluoride nanofibers. *Small*. 2021;17(36):e2102550. doi:10.1002/smll.202102550
18. O'Brien WD Jr. Ultrasound-biophysics mechanisms. *Prog Biophys Mol Biol*. 2007;93(1–3):212–255. doi:10.1016/j.pbiomolbio.2006.07.010
19. Xin Z, Lin G, Lei H, et al. Clinical applications of low-intensity pulsed ultrasound and its potential role in urology. *Transl Androl Urol*. 2016;5(2):255–266. doi:10.21037/tau.2016.02.04
20. Higgins A, Glover M, Yang Y, et al. EXOGEN ultrasound bone healing system for long bone fractures with non-union or delayed healing: a NICE medical technology guidance. *Appl Health Econ Health Policy*. 2014;12(5):477–484. doi:10.1007/s40258-014-0117-6
21. Jiang X, Savchenko O, Li Y, et al. A review of low-intensity pulsed ultrasound for therapeutic applications. *IEEE Trans Biomed Eng*. 2019;66(10):2704–2718. doi:10.1109/tbme.2018.2889669
22. Stride E, Saffari N. The potential for thermal damage posed by microbubble ultrasound contrast agents. *Ultrasonics*. 2004;42(1–9):907–913. doi:10.1016/j.ultras.2003.12.014
23. Celikkin N, Presutti D, Maiullari F, et al. Combining rotary wet-spinning biofabrication and electro-mechanical stimulation for thein vitro production of functional myo-substitutes. *Biofabrication*. 2023;15(4):045012. doi:10.1088/1758-5090/ace934
24. Sharma S, Chhetry A, Sharifuzzaman M, et al. Wearable capacitive pressure sensor based on mxene composite nanofibrous scaffolds for reliable human physiological signal Acquisition. *ACS Appl Mater Interfaces*. 2020;12(19):22212–22224. doi:10.1021/acsami.0c05819
25. Lee JC, Suh IW, Park CH, et al. Polyvinylidene fluoride/silk fibroin-based bio-piezoelectric nanofibrous scaffolds for biomedical application. *J Tissue Eng Regen Med*. 2021;15(10):869–877. doi:10.1002/term.3232
26. Morali A, Mandal A, Skorobogatiy M, et al. Unleashing the piezoelectric potential of PVDF: a study on phase transformation from gamma (γ) to beta (β) phase through thermal contact poling. *RSC Adv*. 2023;13(44):31234–31242. doi:10.1039/d3ra05068h
27. Wang J, Xia Z, Yao H, et al. Self-powered TENG with high humidity sensitivity from PVA Film Modified by LiCl and MXene. *ACS Appl Mater Interfaces*. 2023;15(40):47208–47220. doi:10.1021/acsami.3c08706

28. Lu Z, Jia C, Yang X, et al. A Flexible TENG based on micro-structure film for speed skating techniques monitoring and biomechanical energy harvesting. *Nanomaterials*. 2022;12(9):1576. doi:10.3390/nano12091576
29. Nair HKR. Microcurrent as an adjunct therapy to accelerate chronic wound healing and reduce patient pain. *J Wound Care*. 2018;27(5):296–306. doi:10.12968/jowc.2018.27.5.296
30. Zhang L, Liu M, Zhang Y, et al. Recent progress of highly adhesive hydrogels as wound dressings. *Biomacromolecules*. 2020;21(10):3966–3983. doi:10.1021/acs.biomac.0c01069
31. Ma X, Bian Q, Hu J, et al. Stem from nature: bioinspired adhesive formulations for wound healing. *J Control Release*. 2022;345:292–305. doi:10.1016/j.jconrel.2022.03.027
32. Roper J, Harrison A, Bass MD, et al. Induction of adhesion-dependent signals using low-intensity ultrasound. *J Vis Exp*. 2012;63:e4024. doi:10.3791/4024
33. Wang YT, Meng XT. A review of the evidence to support electrical stimulation-induced vascularization in engineered tissue. *Regen Ther*. 2023;24:237–244. doi:10.1016/j.reth.2023.07.005
34. Fan B, Guo Z, Li X, et al. Electroactive barium titanate coated titanium scaffold improves osteogenesis and osseointegration with low-intensity pulsed ultrasound for large segmental bone defects. *Bioact Mater*. 2020;5(4):1087–1101. doi:10.1016/j.bioactmat.2020.07.001
35. Wu Y, Yu Q, Zhou X, et al. MXene-coated piezoelectric poly-L-lactic acid membrane accelerates wound healing by biomimicking low-voltage electrical pulses. *Inter J Biol Macromol*. 2024;278:134971. doi:10.1016/j.ijbiomac.2024.134971
36. Yang F, Xue Y, Wang F, et al. Sustained release of magnesium and zinc ions synergistically accelerates wound healing. *Bioact Mater*. 2023;26:88–101. doi:10.1016/j.bioactmat.2023.02.019
37. van Nie L, Salinas-Tejedor L, Dychus N, et al. Dopamine induces in vitro migration of synovial fibroblast from patients with rheumatoid arthritis. *Sci Rep*. 2020;10(1):11928. doi:10.1038/s41598-020-68836-z
38. Maleki A, He J, Bochani S, et al. Multifunctional photoactive hydrogels for wound healing acceleration. *ACS Nano*. 2021;15(12):18895–18930. doi:10.1021/acsnano.1c08334
39. Mao H, Zhao S, He Y, et al. Multifunctional polysaccharide hydrogels for skin wound healing prepared by photoinitiator-free crosslinking. *Carbohydr Polym*. 2022;285:119254. doi:10.1016/j.carbpol.2022.119254
40. Hesketh M, Sahin KB, West ZE, et al. Macrophage phenotypes regulate scar formation and chronic wound healing. *Int J Mol Sci*. 2017;18(7):1545. doi:10.3390/ijms18071545
41. Radu P, Brătucu M, Garofil D, et al. The role of collagen metabolism in the formation and relapse of incisional hernia. *Chirurgia*. 2015;110 (3):224–230.